

Supporting information

Design Rules for the Preparation of Low-Cost Hole Transporting Materials for Perovskite Solar Cells with Moisture Barrier Properties

Michiel L. Petrus,¹ Arif Music,¹ Anna C. Closs,¹ Johan C. Bijleveld,² Maximilian T. Sirtl,¹ Yinghong Hu,¹ Theo J. Dingemans,^{2,3} Thomas Bein,¹ Pablo Docampo^{1,4}

¹ Department of Chemistry and Center for NanoScience (CeNS), University of Munich (LMU)
Butenandtstr. 11, 81377 Munich, Germany

² Delft University of Technology, Faculty of Aerospace Engineering, Kluyverweg 1, 2629 HS Delft, The Netherlands.

³ University of North Carolina, Department of Applied Physical Sciences, 1113 Murray Hall, Chapel Hill, NC 27599-3050, USA

⁴ Newcastle University, School of Electrical and Electronic Engineering, NE1 7RU Newcastle upon Tyne, UK

Table of Contents

1	Materials and Methods.....	4
1.1	Synthesis	4
1.1.1	Synthesis of 4,4'-dimethoxy-4''-nitrotriphenylamine.....	4
1.1.2	Synthesis of 4,4'-dimethoxy-4''-aminotriphenylamine	5
1.1.3	General synthesis of hole transporting materials.....	5
1.1.4	NMR and FTIR data interpretation.....	9
1.2	Analytics	9
1.2.1	X-ray diffraction	9
1.2.2	Solar cell characterization.....	10
1.2.3	Cyclic voltammetry.....	10
1.2.4	Thermal characterization	10
1.2.5	Photoluminescence.....	10
1.2.6	External quantum efficiency	10
1.3	Film preparation for hydration studies.....	11
1.3.1	Hydration studies	11
1.4	Solar cell preparation.....	11
1.5	Hole only device preparation.....	11
1.6	Conductivity measurements	12
1.7	Density measurements	12
2	Cost estimation	13
2.1	Waste and Environment	13
2.2	4-amino-4',4''-dimethoxytriphenylamine.....	14
2.2.1	Halogen free synthetic route for 4-amino-4',4''-dimethoxytriphenylamine.....	14
2.2.2	Low cost synthetic route for 4-amino-4',4''-dimethoxytriphenylamine	15
2.3	4-formyl-4',4''-dimethoxytriphenylamine	16
2.4	Ph-OMeTPA.....	17
2.5	Th-OMeTPA.....	18
2.6	Fu-OMeTPA.....	19
2.8	TPA-OMeTPA.....	20
2.9	Ph-inv-OMeTPA.....	21
2.10	Diazo-OMeTPA.....	22
3	Thermal properties	23

4	Optoelectronic properties	25
4.1	UV-Vis spectroscopy	25
4.1.1	Oxidation with LiTFSI.....	26
4.2	Cyclic voltammetry.....	27
4.3	Computational studies.....	27
5	Hole mobility.....	28
6	Solar cell performance	30
7	Moisture barrier properties	33
8	References	37

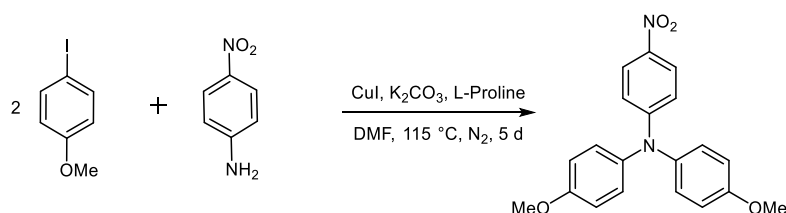
1 Materials and Methods

1.1 Synthesis

All chemicals were purchased from commercial sources and used as received unless stated otherwise.

The structures were confirmed by $^1\text{H-NMR}$ (Bruker spectrometer Avance III, 400 MHz or Jeol 400 MHz) and $^{13}\text{C-NMR}$ (Bruker spectrometer Avance III 100 MHz or Jeol 100 MHz). All samples were dissolved in deuterated solvents and the recorded spectra were referenced to the solvent (CDCl_3 : ^1H , 7.26 and ^{13}C 77.0 ppm C_6D_6 : 7.36 ppm) relative to TMS. Infrared spectra were obtained with a PerkinElmer FT-infrared Spectrometer Paragon 1000 and UV-Vis spectra were collected using a PerkinElmer Lambda 1050 spectrometer. LRMS and HRMS measurements were carried out using a JMS GCmate II jeol applying the FAB+ and on a Thermo Finnigan LTQ FT Ultra applying the ESI method.

1.1.1 Synthesis of 4,4'-dimethoxy-4''-nitrotriphenylamine



Copper(I)iodide (3.43 g, 18.0 mmol), potassium carbonate (77.3 g, 560 mmol) and *L*-proline (6.7 g, 58.0 mmol) were dissolved in 100 mL of DMF. 4-Nitroaniline (9.9 g, 72 mmol) and 4-iodoanisole (54 g, 240 mmol) were dissolved in another 100 mL of DMF and slowly added *via* a syringe. The reaction was then heated to 115 °C under vigorous stirring. After five days the reaction mixture was poured in water (1000 mL) and extracted with ethyl acetate. The organic phase was washed with brine (twice 500 mL). After drying over magnesium sulphate the solvent was removed under vacuum. Crystallisation from diethyl ether, resulted in bright orange crystals in a yield of 63% (15.58 g, 45.2 mmol).

Characterization in agreement with literature. ^[S1]

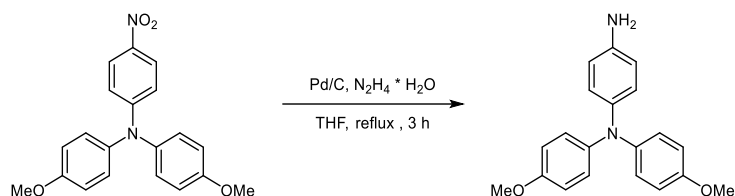
$^1\text{H-NMR}$ (CDCl_3 , 400MHz) δ = 7.97 (d, J = 9.3 Hz, 2H); 7.13 (d, J = 8.9 Hz, 4H); 6.90 (d, J = 8.9 Hz, 4H); 6.75 (d, J = 9.3 Hz, 2H); 3.81 (s, 6H) ppm;

$^{13}\text{C-NMR}$ (CDCl_3 , 100MHz) δ = 157.6; 154.1; 138.9; 138.2; 128.0; 125.4; 115.6; 115.1; 55.4 ppm;

FTIR: $\nu(\text{cm}^{-1})$: 3041, 2841, 1583, 1493, 1236, 1105, 830, 748, 691;

GCMS: m/z (relative intensity): t_R = 20.6 min, 450.0 (100), 335.0 (58), 289.0 (25), 351.0 (21), 336.0 (12), 77.1 (12)

1.1.2 Synthesis of 4,4'-dimethoxy-4''-aminotriphenylamine



6.16 g of compound **1** (17.6 mmol) was dissolved in 80 mL THF. 0.2 g of palladium on carbon was mixed with 2 mL of THF and added slowly to the solution. The mixture was heated to reflux (it is important to heat to reflux before adding the hydrazine) and 6 g hydrazine solution (66% in water) in 20 mL THF was added slowly via a dropping funnel over one hour. After addition, the reaction was refluxed for two more hours. After cooling down to room temperature, the palladium on carbon was removed *via* filtration under nitrogen and the volume was reduced. Upon addition of water the product precipitates, was filtered off as a clear white powder and was dried under vacuum (5.2 g, 16.2 mmol, 92%).

Characterization in agreement with literature.^[S1]

¹H-NMR (CDCl₃, 400MHz) δ: 6.98 (d, *J* = 8.9 Hz, 4H); 6.90 (d, *J* = 8.6 Hz, 2H); 6.79 (d, *J* = 9.0 Hz, 4H); 6.59 (d, *J* = 8.7 Hz, 2H); 3.78 (s, 6H); 3.58 (s, broad, 2H) ppm;

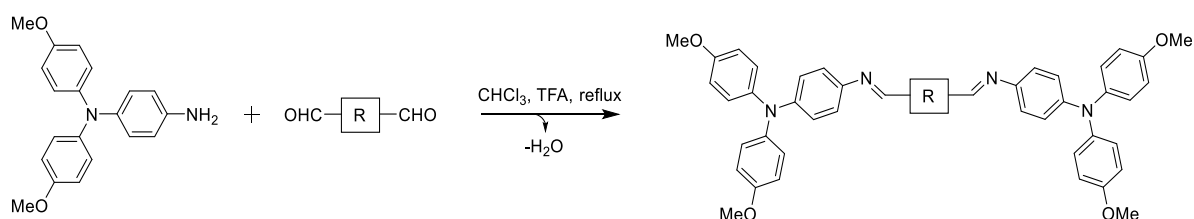
¹³C-NMR (CDCl₃, 100MHz) δ: 154.4; 142.1; 414.6; 139.9; 125.5; 124.1; 115.9; 114.3; 55.3 ppm;

FTIR: ν(cm⁻¹): 3457, 3373, 3033, 2836, 1634, 1497, 1232, 1027, 817;

MS *m/z* (relative intensity): 320.0 (100), 305.0 (63), 321.1 (20), 160.0 (18), 306.0 (13)

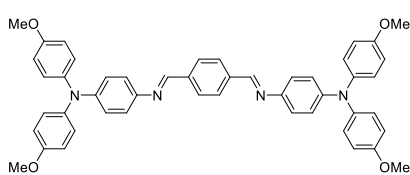
1.1.3 General synthesis of hole transporting materials

EDOT-OMeTPA and Diazo-OMeTPA were synthesized according to literature (density 1.24 g cm⁻³).^[S2, S3]



4,4'-dimethoxy-4''-aminotriphenylamine (2.40 eq) and the dialdehyde (1.00 eq) were dissolved in 40 mL dry chloroform. After addition of one drop of trifluoroacetic acid the mixture was refluxed for 4 hours. After cooling down to R.T. the reaction mixture was slowly poured into an isopropanol/hexane solution (250 mL), which also contained 0.5 mL of trimethylamine to neutralize the acid and the azomethine bond. The precipitate was obtained *via* filtration and additionally washed twice with an isopropanol/hexane solution. The products were dried under vacuum at elevated temperature.

1.1.3.1 Ph-OMeTPA



4,4'-dimethoxy-4''-aminotriphenylamine (0.890 g, 2.78 mmol) and isophthalaldehyde (0.160 g, 1.16 mmol), yield = 0.830 g (1.12 mmol, 97%).

Orange powder, $R_f = 0.25$ (DCM);

$^1\text{H-NMR}$ (400 MHz, CDCl_3) $\delta = 8.53$ (s, 2H), 7.96 (s, 4H), 7.21 – 7.15 (m, 4H), 7.10 – 7.04 (m, 8H), 6.99 – 6.94 (m, 4H), 6.87 – 6.81 (m, 8H), 3.80 (s, 12H) ppm;

$^1\text{H-NMR}$ (400 MHz, C_6D_6) $\delta = 8.31$ (s, 2H), 7.92 (s, 4H), 7.33 – 7.27 (m, 4H), 7.19 – 7.11 (m, 12H), 6.81 – 6.74 (m, 8H), 3.34 (s, 12H) ppm;

$^{13}\text{C-NMR}$ (101 MHz, CDCl_3) $\delta = 156.4, 155.9, 147.7, 144.7, 141.2, 140.9, 128.8, 126.5, 122.1, 121.2, 114.7, 55.5$ ppm;

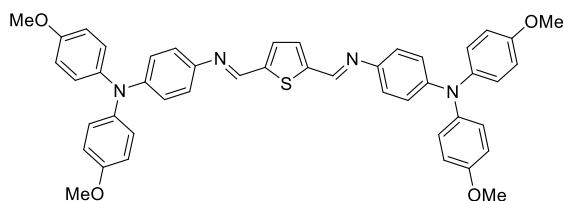
$^{13}\text{C-NMR}$ (101 MHz, C_6D_6) $\delta = 156.2, 156.0, 147.8, 144.8, 141., 138.9, 128.8, 126.5, 122.4, 121.6, 114.9, 54.7$ ppm;

LRMS (FAB pos): m/z (%) = 739.0 (68), 460.6 (30), 307.5 (100), 289.4 (94), 155.3 (100), 107.2 (91), 65.2 (22);

HRMS (FAB pos): m/z calcd for $\text{C}_{48}\text{H}_{42}\text{N}_4\text{O}_4^+$ $[\text{M}+\text{H}]^+$: 739.3279; found: 739.3298;

FTIR: $\nu(\text{cm}^{-1})$: 3000 (w), 2947 (w), 2832 (w), 1618 (m), 1586 (w), 1502 (s), 1462 (m), 1441 (m), 1315 (m), 1284 (m), 1272 (m), 1235 (s), 1178 (m), 1107 (m), 1032 (s), 830 (s);

1.1.3.2 Th-OMeTPA



4,4'-dimethoxy-4''-aminotriphenylamine (2.00 g, 6.25 mmol) and 2,5-thiophenedicarboxaldehyde (0.365 g, 2.60 mmol), yield = 1.70 g (2.28 mmol, 88%).

Red powder, $R_f = 0.53$ (DCM);

$^1\text{H-NMR}$ (400 MHz, CDCl_3) $\delta = 8.57$ (s, 2H), 7.41 (s, 2H), 7.16 (m, 4H), 7.09 – 7.03 (m, 8H), 6.97 – 6.91 (m, 4H), 6.86 – 6.80 (m, 8H), 3.80 (s, 12H) ppm;

$^1\text{H-NMR}$ (400 MHz, C_6D_6) $\delta = 8.26$ (s, 2H), 7.23 – 7.04 (m, 12H), 6.97 (s, 4H), 6.80 – 6.69 (m, 2H), 5.41 (s, 8H), 3.31 (s, 12H) ppm;

$^{13}\text{C-NMR}$ (101 MHz, CDCl_3) $\delta = 155.9, 149.1, 147.8, 143.3, 140.8, 130.9, 126.8, 126.5, 122.2, 121.1, 114.7, 55.5$ ppm;

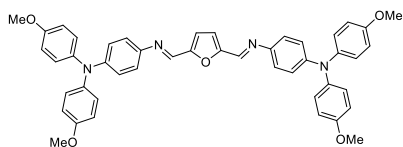
$^{13}\text{C-NMR}$ (101 MHz, C_6D_6) $\delta = 156.2, 148.9, 147.9, 146.8, 143.9, 141.1, 130.5, 126.5, 122.6, 121.4, 114.8, 54.7$ ppm;

LRMS (FAB pos): m/z (%) = 744.9 (82), 460.6 (7), 307.5 (62), 154.3 (100), 136.3 (97);

HRMS (FAB pos): m/z calcd for $\text{C}_{46}\text{H}_{40}\text{N}_4\text{O}_4\text{S}^+$ $[\text{M}+\text{H}]^+$: 745.2843; found: 745.2856;

FTIR: $\nu(\text{cm}^{-1})$: 2930 (w), 2831 (w), 1605 (m), 1500 (s), 1461 (m), 1440 (w), 1317 (w), 1280 (m), 1229 (s), 1178 (m), 1104 (w), 1033 (m), 828 (s);

1.1.3.3 Fu-OMeTPA



4,4'-dimethoxy-4''-aminotriphenylamine (0.50 g, 1.56 mmol) and 2,5-furandicarboxaldehyde (0.097 g, 0.78 mmol) were used in a stoichiometric ratio, yield = 0.46 g (0.63 mmol, 81%);

Red powder, $R_f = 0.87$ (DCM);

$^1\text{H-NMR}$ (400 MHz, CDCl_3) $\delta = 8.43$ (s, 2H), 7.21 – 7.15 (m, 4H), 7.11 – 7.03 (m, 10H), 6.97 – 6.91 (m, 4H), 6.87 – 6.80 (m, 8H), 3.80 (s, 12H) ppm;

$^1\text{H-NMR}$ (400 MHz, C_6D_6): $\delta = 8.20$ (s, 2H), 7.23 – 7.21 (m, 4H), 7.10 – 7.06 (m, 12H), 6.81 (s, 2H), 6.75 – 6.71 (m, 8H), 3.31 (s, 12H) ppm;

$^{13}\text{C-NMR}$ (101 MHz, CDCl_3) $\delta = 156.0, 154.5, 148.1, 144.4, 143.1, 140.7, 126.7, 122.2, 120.7, 115.5, 114.8, 55.5$ ppm;

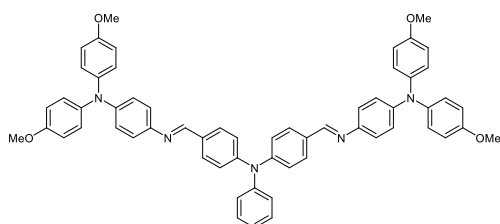
$^{13}\text{C-NMR}$ (101 MHz, C_6D_6): $\delta = 156.3, 155.0, 148.1, 144.1, 144.1, 141.0, 126.6, 122.43, 121.3, 114.8, 114.6, 54.7$ ppm;

LRMS (FAB pos): m/z (%) = 728.9 (94), 727.9 (6), 622.0 (3), 460.6 (5), 307.5 (44), 154.3 (100), 136.3 (92);

HRMS (FAB pos): m/z calcd for $\text{C}_{46}\text{H}_{40}\text{N}_4\text{O}_5^+$ $[\text{M}+\text{H}]^+$: 729.3071; found: 729.3068;

FTIR: $\nu(\text{cm}^{-1})$: 2950 (w), 2832 (w), 1615 (m), 1581 (w), 1501 (s), 1462 (m), 1440 (w), 1317 (w), 1280 (m), 1237 (s), 1179 (m), 1160 (w), 1105 (w), 1032 (m), 825 (s).

1.1.3.4 TPA-OMeTPA



4,4'-dimethoxy-4''-aminotriphenylamine (1.00 g, 3.13 mmol) and triphenylamino-4,4'-dicarboxaldehyde (0.392 g, 1.30 mmol), yield = 1.12 g (1.24 mmol, 95%).

Yellow powder, $R_f = 0.47$ (DCM);

$^1\text{H-NMR}$ (400 MHz, CDCl_3) $\delta = 8.42$ (s, 2H), 7.76 (m, 4H), 7.36 – 7.30 (m, 2H), 7.20 – 7.09 (m, 11H), 7.09 – 7.03 (m, 8H), 6.99 – 6.94 (m, 4H), 6.86 – 6.80 (m, 8H), 3.80 (s, 12H) ppm;

$^1\text{H-NMR}$ (400 MHz, C_6D_6) $\delta = 8.30$ (s, 2H), 7.79 – 7.73 (m, 4H), 7.30 – 7.23 (m, 4H), 7.15 – 7.09 (m, 13H), 7.07 – 7.01 (m, 8H), 6.76 – 6.71 (m, 8H), 3.32 (s, 12H) ppm;

$^{13}\text{C-NMR}$ (101 MHz, CDCl_3) $\delta = 156.8, 155.7, 149.6, 147.1, 146.5, 144.9, 141.1, 131.3, 129.9, 129.7, 129.7, 126.2, 126.0, 123.4, 121.8, 121.7, 114.7, 55.5$ ppm;

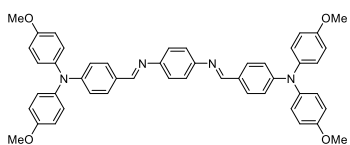
¹³C-NMR (101 MHz, C₆D₆) δ = 156.1, 156.0, 149.5, 147.3, 146.8, 145.6, 141.4, 131.9, 129.9, 129.5, 126.3, 125.7, 124.3, 123.4, 122.2, 122.1, 114.8, 54.7 ppm;

LRMS (ESI 70 eV): m/z (%) = 906.4 (94), 822.5 (49), 527.1 (9), 306.1 (47), 267.0 (60), 213.5 (100);

HRMS (ESI): m/z calcd for C₆₀H₅₁N₅O₄⁺ [M+H]⁺: 906.4014; found: 906.4021;

FTIR: ν(cm⁻¹): 3032 (w), 2929 (w), 2830 (w), 1616 (m), 1593 (w), 1504 (s), 1462 (m), 1439 (m), 1314 (m), 1271 (m-br), 1234 (s), 1165 (s), 1103 (m), 1032 (s), 823 (s);

1.1.3.5 Ph-inv-OMeTPA



4,4'-dimethoxy-4''-formyltriphenylamine (1.16 g; 3.48 mmol; 2.5 eq) and the benzene-1,4-diamine (0.15 g; 1.40 mmol; 1.00 eq) were dissolved in 20 mL dry chloroform. After addition of one drop of trifluoroacetic acid the mixture was refluxed for 4 hours. After cooling down to R.T. the reaction mixture was slowly poured into isopropanol, which also contained trimethylamine to neutralize the acid and the azomethine bond. The precipitate was obtained *via* filtration and additionally washed with ethanol. The product was dried under vacuum, the title compound was obtained as a dark orange solid (0.85 g; 1.15 mmol; 82%).

¹H-NMR (400 MHz, CDCl₃) δ = 8.35 (s, 2H), 7.66 (d, ³J = 8.1 Hz, 4H), 7.20 (s, 4H), 7.09 (d, ³J = 9.0 Hz, 8H), 6.90 (d, ³J = 8.6 Hz, 4H), 6.85 (d, ³J = 9.0 Hz, 8H), 3.79 (s, 12H)

¹H-NMR (400 MHz, C₆D₆): δ = 8.29 (s, 2H), 7.86 (d, ³J = 8.8 Hz, 4H), 7.29 (s, 4H), 7.09-7.04 (m, 12H), 6.71 (d, ³J = 9.2 Hz, 8H), 3.30 (s, 12H) ppm;

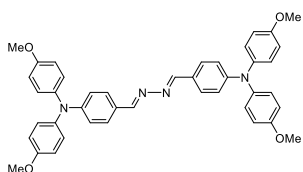
¹³C-NMR (101 MHz, C₆D₆): δ = 158.3, 157.2, 151.8, 150.8, 140.5, 130.5, 129.3, 127.7, 122.4, 119.3, 115.3, 55.1 ppm;

LRMS (FAB pos): m/z (%) = 739.9 (98), 738.9 (91), 408.6 (5), 307.5 (15), 154.3 (46), 136.3 (26);

HRMS (FAB pos): m/z calcd for C₄₈H₄₂N₄O₄⁺ [M+H]⁺: 738.3206; found: 738.3250;

FTIR: ν(cm⁻¹): 2930 (w), 2832 (w), 1592 (s), 1558 (w), 1500 (s), 1462 (w), 1440 (w), 1430 (w), 1319 (w), 1280 (m), 1237 (s), 1187 (w), 1160 (s), 1104 (m), 1031 (s), 824 (s)

1.1.3.6 Diazo-OMeTPA



Synthesis is described in literature.^[S14]

¹H-NMR (400 MHz, CDCl₃) δ = 8.54 (s, 2H), 7.59 (d, ³J = 8.8 Hz, 4H), 7.10 (d, ³J = 9.2 Hz, 8H), 6.89 (d, ³J = 8.8 Hz, 4H), 6.86 (d, ³J = 9.2 Hz, 8H), 3.81 (s, 12H)

¹³C-NMR (101 MHz, DMSO-d₆): δ = 160.8, 156.6, 151.2, 139.9, 129.4, 127.4, 125.6, 118.7, 114.8, 55.5 ppm;

FTIR: ν(cm⁻¹): 1610 (m), 1597 (m), 1470 (s), 1240 (s), 1168 (s), 1033 (s)

Density: 1.27 g cm⁻³

1.1.4 NMR and FTIR data interpretation

Table S 1. NMR and FTIR data from the azomethine bond.

Compound	δ (ppm, ^1H NMR)	ν (nm, FTIR $-\text{HC}=\text{N}-$ stretching)
EDOT-OMeTPA	8.60	1603
Ph-OMeTPA	8.53	1618
Th-OMeTPA	8.57	1605
Fu-OMeTPA	8.43	1615
TPA-OMeTPA	8.42	1616
Ph-inv-OMeTPA	8.35	1592
Diazo-OMeTPA	8.54	1610

The NMR chemical shift and vibrational frequency of the azomethine bond. A down-field shift in the NMR signal indicates an increase in the conjugation of the azomethine-bond. Similarly, lower wavenumbers indicate more conjugation through the azomethine-bond.

1.2 Analytics

1.2.1 X-ray diffraction

X-ray diffraction (XRD) analysis of perovskite films was carried out in reflection mode using a Bruker D8 Discover diffractometer with Ni-filtered Cu $K\alpha_1$ -radiation ($\lambda = 1.5406 \text{ \AA}$) and a position-sensitive semiconductor detector (LynxEye).

For the *in-situ* XRD measurements during the hydration process, a custom-made hydration chamber made of X-ray transparent polymers with a total volume of around 250 mL was utilized. The air humidity within the hydration chamber was measured using a hygrometer and was held constant at around 90% RH by employing vials filled with salt solution. All experiments were performed at room temperature ($24 \pm 2 \text{ }^\circ\text{C}$) without illumination.

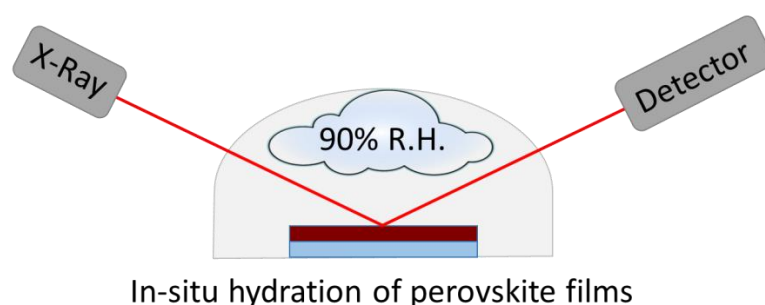


Figure S 1. Schematic representation of the hydration chamber.^[S4]

1.2.2 Solar cell characterization

J-V curves of solar cells were recorded under ambient conditions with a Keithley 2400 source meter under simulated AM 1.5G sunlight, with an incident power of approximately 100 mW cm^{-2} , which was corrected for the exact light intensity using a Fraunhofer ISE certified silicon cell. The active area of the solar cells was defined with a square metal aperture mask of 0.0831 cm^2 . The reported device characteristics were estimated from the measured *J-V* curves obtained from the reverse scan (from V_{oc} to J_{sc}) which was recorded at a scan rate of 0.2 V s^{-1} after pre-biasing at 1.5 V for 5 s under illumination. All as-prepared devices show a comparable degree of hysteresis between the forward and reverse scan.

1.2.3 Cyclic voltammetry

Cyclic voltammetry (CV) experiments were performed using a Metrohm Potentiostat (PGSTAT302N) with platinum working and counter electrode and an Ag/AgCl reference electrode. Experiments were performed in anhydrous and degassed dichloromethane solutions of the hole transporter with 0.1 M tetrabutylammonium hexafluorophosphate ($t\text{BuNPF}_6$) as electrolyte and a scan rate of 100 mV s^{-1} . HOMO levels were calculated according to literature (the formal potential of the Fc^+/Fc redox couple used is -5.1 eV).^[S2]

1.2.4 Thermal characterization

Thermogravimetric analysis (TGA) was performed using a Netzsch STA 449 C Jupiter under nitrogen atmosphere with a scan rate of $10 \text{ }^\circ\text{C min}^{-1}$. Differential scanning calorimetry (DSC) was performed under nitrogen atmosphere using a Perkin Elmer DSC8000 at a heating rate of $20 \text{ }^\circ\text{C min}^{-1}$. Melting behaviour was confirmed using a melting point apparatus.

1.2.5 Photoluminescence

PL measurements were performed with a Fluotime 300 Spectrofluorometer (Picoquant GmbH). The excitation wavelength was fixed at 510 nm. The emission for time resolved measurements was monitored at the maximum intensity if the steady state photo emission.

1.2.6 External quantum efficiency

External quantum efficiency measurements were performed at short-circuit and referenced to a Si photodiode (Hamamatsu). The device was illuminated using a white bias light (Solar light Co. Inc. Model S16, 150W xenon lamp $\sim 100 \text{ W m}^{-2}$) and light from a 150 W Xe short arc lamp (LOT Oriel) was used as probe light and modulated with a mechanical chopper (12 Hz) and passed through a monochromator (Horiba MicroHR) to select the wavelength. The response was recorded using a lock-in amplifier (Ametek Signal Recovery SR 7230 DSP) with a low-noise pre-amplifier (Femto DLPCA-200).

1.3 Film preparation for hydration studies

Microscopy glass substrates (2.5 x 2.5 cm) were successively cleaned with a 2% Hellmanex solution and rinsed with de-ionized water, ethanol and acetone. Directly before spin-coating the perovskite film, the substrates were plasma cleaned for 5 min. A precursor solution containing 1.31 M PbI_2 (TCI, >98%) and 1.25 M methylammonium iodide (Dyesol) in a *N,N*-dimethylformamide (DMF) : dimethyl sulfoxide (DMSO) solvent mixture (1:4 vol/vol) was prepared. The solutions were spin-coated dynamically (first at 1000 rpm for 10 s, followed by a second step at 5000 rpm for 30 s) onto the substrate. After 25 s, chlorobenzene was added on top of the spinning substrate and afterwards the substrate was annealed on a hotplate (first at 40 °C for 40 min, followed by a second step at 100 °C for 10 min). The hole transporting material spiro-OMeTAD (Borun Chemicals, 99.5% purity) was applied on the perovskite film using a 75 mg/mL solution in chlorobenzene, while the azomethine-based HTMs were spincoated from a 10 mg/mL solution in chlorobenzene. To all HTM solutions 10 $\mu\text{L}/\text{mL}$ 4-*tert*-butylpyridine (*t*BP) and 30 $\mu\text{L}/\text{mL}$ of a 170 mg/mL bis(trifluoromethane)sulfonamide lithium salt (LiTFSI) solution in acetonitrile were added. The HTM solutions were spin-coated dynamically at 1500 rpm for 45 s.

1.3.1 Hydration studies

For hydration studies the edges of the substrates were first covered with epoxy for the samples with the epoxy covered edge. All samples were allowed to oxidize overnight at <30% R.H, before they were placed in an exicator with a R.H. of 75% which was held constant using salt solutions and monitored using a hygrometer. The desiccator was closed with a glass plate that allows taking photos without removing the lid, in order to reduce fluctuations in the humidity. The exicator was stored in the dark to prevent light induced degradation.

1.4 Solar cell preparation

Fluorine-doped tin oxide (FTO) coated glass sheets (7 Ω/sq , Pilkington, USA) were patterned and cleaned. Directly before applying the hole-blocking layer the substrates were plasma cleaned. A compact TiO_2 layer was prepared from a sol-gel precursor solution by spin-coating onto the substrates and calcination at 500 °C for 30 min in air. For the sol-gel solution a 27.2 mM solution of HCl in 2-propanol was added dropwise to a vigorously stirred 0.43 mM solution of titanium isopropoxide (99.999 %, Sigma-Aldrich) in dry 2-propanol. After cooling down, the substrate was transferred to a nitrogen-filled glovebox. The perovskite films and HTM layers were prepared as described above. The devices were stored overnight under air at room temperature and < 30% RH to allow the hole transporting materials to oxidize. The top electrode with a thickness of 40 nm was deposited by thermal evaporation of gold under vacuum (at $\sim 10^{-6}$ mbar).

1.5 Hole only device preparation

ITO-substrates (1.5 x 2.0 cm, VisionTek, 12 Ω/sq to 15 Ω/sq) were etched and cleaned. The substrates were plasma cleaned prior to the thermal deposition of the MoO_x layer (10 nm) under vacuum ($\sim 1 \cdot 10^{-6}$ mbar). The substrates were exposed to air and stored in a nitrogen-filled glovebox. Next, the layers of HTMs were spincoated from chlorobenzene at a concentration of 10 mg mL^{-1} , resulting in a thickness of 40-60 nm. A top electrode of MoO_x (10 nm), followed by a layer of gold

(100 nm) was deposited under vacuum ($1 \cdot 10^{-6}$ mbar). The active area was 16 mm^2 . Current-voltage characteristics were recorded in air in the dark using a Metrohm potentiostat (PGSTAT302N) at a scan rate of 0.1 V s^{-1} . The layer thickness was determined by using atomic force microscopy (AFM) measurements, which were performed in tapping mode using a NanoInk DPN Stage microscope, or with a Veeco Dektak 150.

1.6 Conductivity measurements

Glass substrates with a thin compact layer of Al_2O_3 were used to improve the wetting of the HTMs on the substrate. The HTMs were spincoated at 1000 rpm from a chlorobenzene solution containing the given amount of LiTFSI as oxidant, resulting in a film thickness of 50 nm. The films were stored for 24 h in a desiccator (< 30% R.H.) before 40 nm thick gold electrodes were thermally deposited under vacuum ($\sim 10^{-6}$ mbar). The electrode pattern was designed for two point probe measurements with a channel length of 250, 500 and 1000 μm , a channel width of 0.2, 0.1 and 0.056 m respectively. No significant differences were observed depending on the electrode pattern and the measured values were averaged over at least 8 individual devices. *J-V* curves were recorded under ambient conditions without illumination using a Keithley 2400 source meter at a scan rate of 1 V s^{-1} in the range from -5 to 5 V.

1.7 Density measurements

The density of the HTMs was determined by spincoating films from chlorobenzene onto silicon substrates. Film thickness was measured using a Dektak 150 surface profiler and averaged over at least three different measurements. The bottom and sides of the substrate were carefully cleaned with acetone, to remove any material that ended there during the spincoating. Additionally the edges of the HTM film were removed with a razorblade and cleaned with acetone, in order to remove any edges where increased film thickness is often observed. Afterwards the area of the film was accurately measured, before re-dissolving the film in a known amount of chlorobenzene. With the area and thickness, the volume of the film is calculated. The light absorption of the obtained solution was measured at the absorption maximum of the HTM using an UV-Vis spectrophotometer. A calibration line using known concentrations of the HTM was prepared in order to determine the concentration of the solution containing the dissolved HTM film using Lambert-Beer's law. From the determined concentration, the mass of the HTM film was calculated. With the volume and mass of the film, the density was calculated.

The density of **EDOT-OMeTAD** was determined to be 1.24 g cm^{-3} , **Diazo-OMeTPA** = 1.27 g cm^{-3} and **Spiro-OMeTAD** 1.03 g cm^{-3} .

2 Cost estimation

The cost estimation was done using our previously published material cost model,^[S2] which was based on the work by Osedach *et al.* The synthetic routes are based on published and peer reviewed synthetic procedures and prices have been taken from Sigma-Aldrich, TCI chemicals and Acros using the largest available package on their websites. The synthetic flow charts and material cost calculations can be found below. The results are summarized in *Table S 2*.

Table S 2. Survey of the estimated material cost and an estimate of the chemicals waste produced.

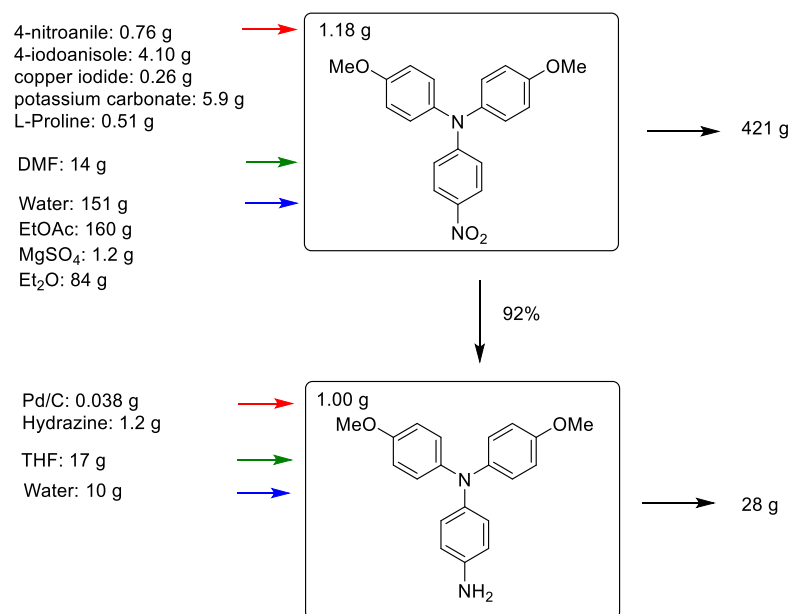
Compound	Material cost (\$ g⁻¹)	Estimated chemical waste (kg g⁻¹)	E Factor (kg waste/kg product)
EDOT-OMeTPA ^[S2]	10	0.7	700
Ph-OMeTPA	4	0.5	500
Th-OMeTPA	7	0.5	500
Fu-OMeTPA	17	0.4	400
TPA-OMeTPA	22	0.5	500
Ph-inv-OMeTPA	32	1.3	1300
Diazo-OMeTPA	54	2.8	2800
Spiro-OMeTAD ^[S2]	92	3.6	3600

2.1 Waste and Environment

The chemical waste for the synthesis was estimated from the synthetic flow charts; the results are summarized in *Table S 2*. We observe that all azomethine-based HTMs require significant less chemicals than Spiro-OMeTAD. Reducing the amount of chemicals is beneficial from a cost point of view as is clear from the material cost, but also regarding the cost involved with chemical waste management. Furthermore, reducing the amount of (toxic) chemicals is beneficial for the environment.

2.2 4-amino-4',4''-dimethoxytriphenylamine

2.2.1 Halogen free synthetic route for 4-amino-4',4''-dimethoxytriphenylamine

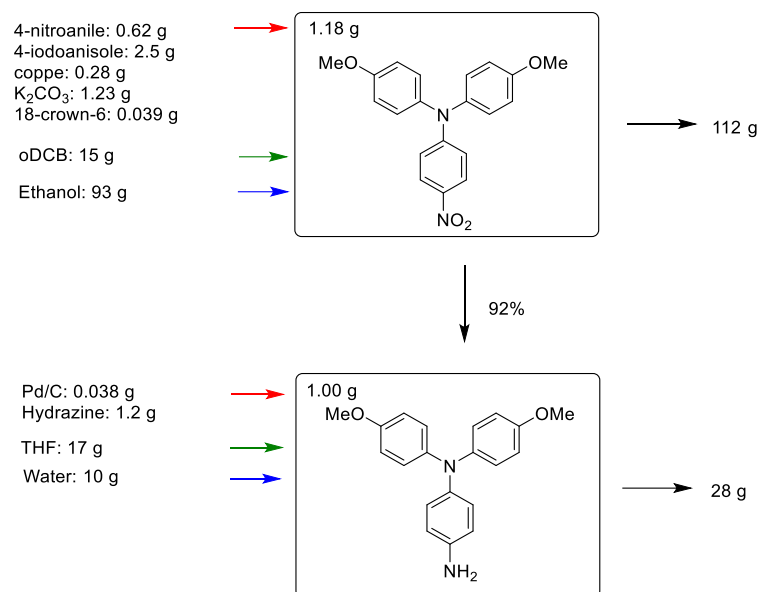


Scheme S 1. Flow chart describing the synthesis of 4-amino-4',4''-dimethoxytriphenylamine as reported in this work. This halogen free synthetic route results in a cost of \$4.70 per gram.

Table S 3. Estimated materials cost for the synthesis of 4-amino-4',4''-dimethoxytriphenylamine.

Chemical name	Price of Chemical (\$/kg)	Material cost (\$/g product)
4-nitroaniline	\$222.60	\$0.17
4-iodoanisole	\$474.18	\$1.94
K ₂ CO ₃	\$6.27	\$0.04
Cu powder	\$61.57	\$0.02
L-proline	\$90.63	\$0.05
DMF	\$5.09	\$0.07
Water	\$0.00	\$0.00
EtOAc	\$3.63	\$0.58
MgSO ₄	\$54.24	\$0.07
Et ₂ O	\$16.57	\$1.39
Hydrazine	\$33.17	\$0.04
Pd/C 10%	\$4,790.10	\$0.18
THF	\$9.24	\$0.16
water	\$0.00	\$0.00
Total	-	\$4.70

2.2.2 Low cost synthetic route for 4-amino-4',4''-dimethoxytriphenylamine

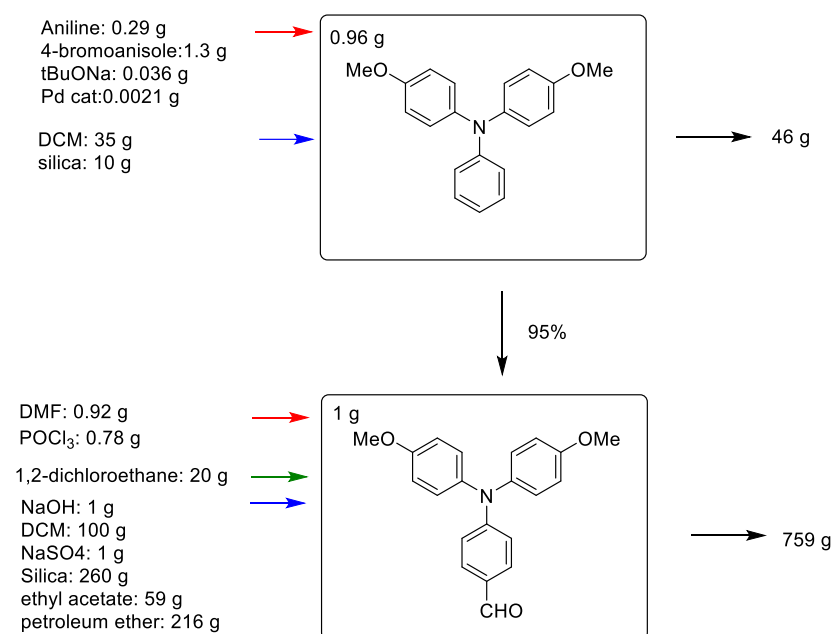


Scheme S 2. Flow chart describing the synthesis of 4-amino-4',4''-dimethoxytriphenylamine using reported synthetic procedures resulting in a minimum cost. This synthetic route results in a cost of \$2.45 per gram for the triphenylamine. However, halogenated solvents are used in this synthetic procedure.^[S5-S6]

Table S 4. Estimated materials cost for the synthesis of 4-amino-4',4''-dimethoxytriphenylamine.

Chemical name	Price of Chemical (\$/kg)	Material cost (\$/g product)
4-nitroaniline	\$222.60	\$0.14
4-iodoanisole	\$474.18	\$1.19
K ₂ CO ₃	\$6.27	\$0.01
Cu powder	\$61.57	\$0.02
18-crown-6-ether	\$2,333.31	\$0.09
oDCB	\$10.46	\$0.16
ethanol	\$3.24	\$0.30
Hydrazine	\$33.17	\$0.04
Pd/C 10%	\$4,790.10	\$0.18
THF	\$9.24	\$0.16
water	\$0.00	\$0.00
Total	-	\$2.28

2.3 4-formyl-4',4''-dimethoxytriphenylamine

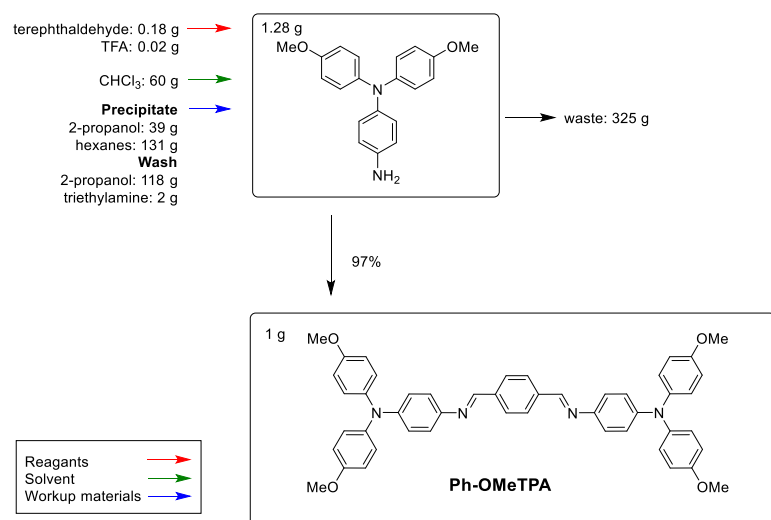


Scheme S 3. Flow chart describing the synthesis of 4-formyl-4',4''-dimethoxytriphenylamine.^[S7-S10]

Table S 5. Estimated materials cost for the synthesis of 4-formyl-4',4''-dimethoxytriphenylamine.^a estimated price.

Chemical name	Price of Chemical (\$/kg)	Material cost (\$/g product)
aniline	\$26.16	0.01
4-bromoanisole	\$109.20	0.20
tBuONa	\$115.74	0.01
Pd cat ^a	\$100,000.00	0.30
DCM	\$11.16	0.56
Silica (short path)	\$66.41	0.90
DMF	\$5.09	0.01
POCl ₃	\$70.35	0.08
1,2-dichloroethane	\$9.96	0.28
NaOH	\$5.38	0.01
water	\$0.00	0.00
DCM	\$11.16	1.56
NaSO ₄	\$12.79	0.02
Silica	\$66.41	24.44
ethyl acetate	\$3.63	0.30
petroleum ether	\$13.95	4.25
Total	-	\$23.31

2.4 Ph-OMeTPA

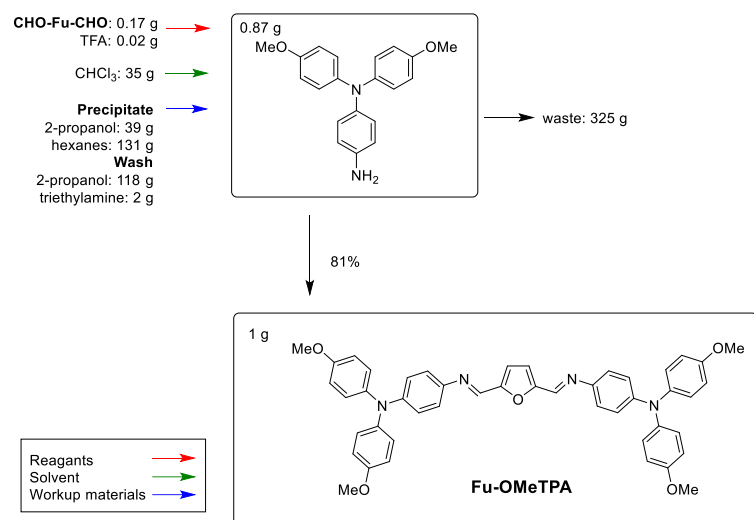


Scheme S 4. Flow chart describing the synthesis of **Ph-OMeTPA**.

Table S 6. *Materials quantities and cost for the synthesis of Ph-OMeTPA.*

Chemical name	Price of Chemical (\$/kg)	Material cost (\$/g product)
terephthalaldehyde	\$233.42	\$0.04
TPA-NH ₂	\$2,280.00	\$2.44
TFA	\$141.12	\$0.00
CHCl ₃	\$2.42	\$0.15
hexane	\$6.31	\$0.83
isopropanol	\$4.18	\$0.16
isopropanol	\$4.18	\$0.49
triethylamine	\$21.54	\$0.04
Total	-	\$4.16

2.6 Fu-OMeTPA

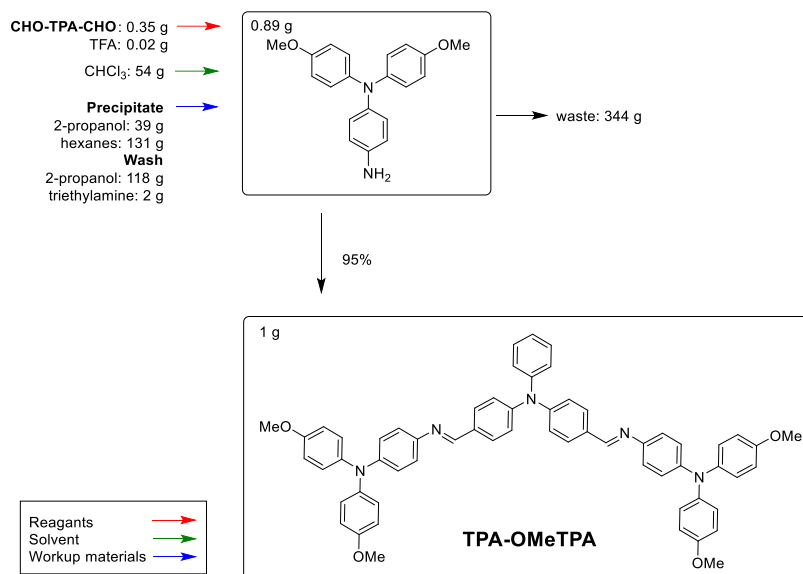


Scheme S 6. Flow chart describing the synthesis of **Fu-OMeTPA**.

Table S 8. Materials quantities and cost for the synthesis of **Fu-OMeTPA**.

Chemical name	Price of Chemical (\$/kg)	Material cost (\$/g product)
2,5-Furandicarboxaldehyde	\$80,535.00	\$13.69
TPA-NH ₂	\$2,280.00	\$1.98
TFA	\$141.12	\$0.00
CHCl ₃	\$2.42	\$0.08
hexane	\$6.31	\$0.83
isopropanol	\$4.18	\$0.16
isopropanol	\$4.18	\$0.49
triethylamine	\$21.54	\$0.04
Total	-	\$17.29

2.8 TPA-OMeTPA

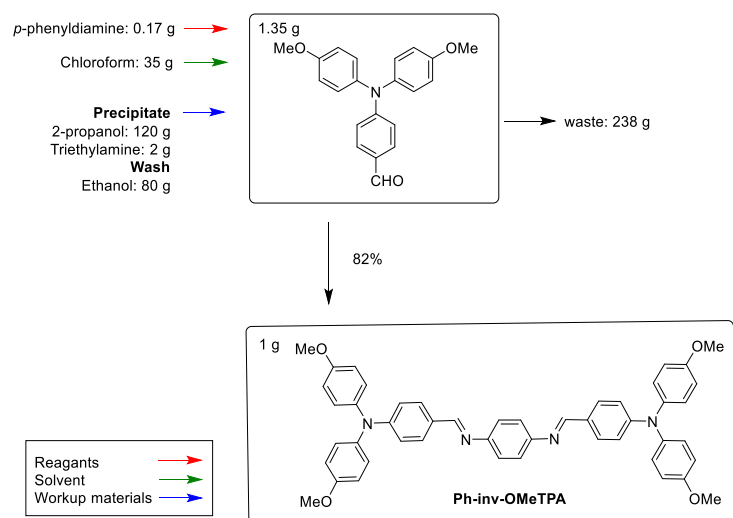


Scheme S 7. Flow chart describing the synthesis of **TPA-OMeTPA**.

Table S 9. Materials quantities and cost for the synthesis of **TPA-OMeTPA**.

Chemical name	Price of Chemical (\$/kg)	Material cost (\$/g product)
4,4'-Diformyltriphenylamine	\$52,689.00	\$18.44
TPA-NH ₂	\$2,280.00	\$2.03
TFA	\$141.12	\$0.00
CHCl ₃	\$2.42	\$0.13
hexane	\$6.31	\$0.83
isopropanol	\$4.18	\$0.16
isopropanol	\$4.18	\$0.49
triethylamine	\$21.54	\$0.04
Total	-	\$22.13

2.9 Ph-inv-OMeTPA

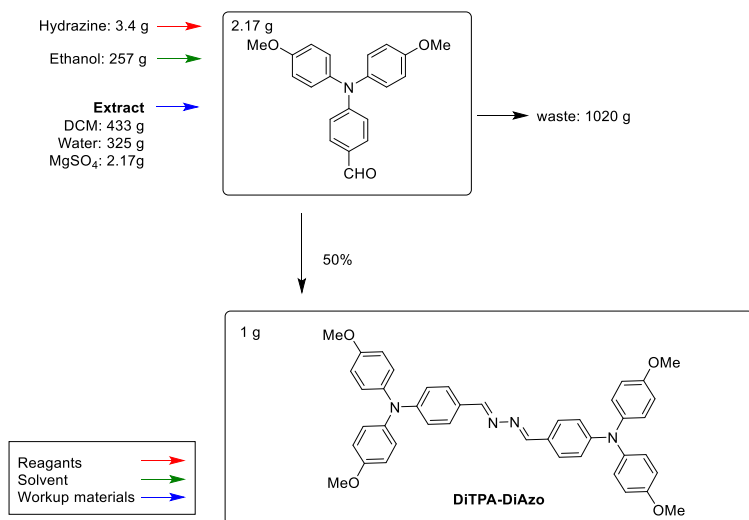


Scheme S 8. Flow chart describing the synthesis of **Ph-inv-OMeTPA**.

Table S 10. Materials quantities and cost for the synthesis of **Ph-inv-OMeTPA**.

Chemical name	Price of Chemical (\$/kg)	Material cost (\$/g product)
TPA-CHO	\$23,310.00	31.47
p -phenylenediamine	\$153.68	\$0.03
CHCl ₃	\$2.42	\$0.08
ethanol	\$3.24	\$0.26
isopropanol	\$4.18	\$0.50
triethylamine	\$21.54	\$0.04
Total	-	\$32.38

2.10 Diazo-OMeTPA



Scheme S 9. Flow chart describing the synthesis of **Diazo-OMeTPA**.

Table S 11. Materials quantities and cost for the synthesis of **Diazo-OMeTPA**.

Chemical name	Price of Chemical (\$/kg)	Material cost (\$/g product)
TPA-CHO	\$23,310.00	\$50.58
hydrazine	\$35.70	\$0.12
ethanol	\$3.48	\$0.89
DCM	\$4.48	\$1.94
Water	\$0.00	\$0.00
MgSO ₄	\$54.24	\$0.12
Total	-	\$53.66

3 Thermal properties

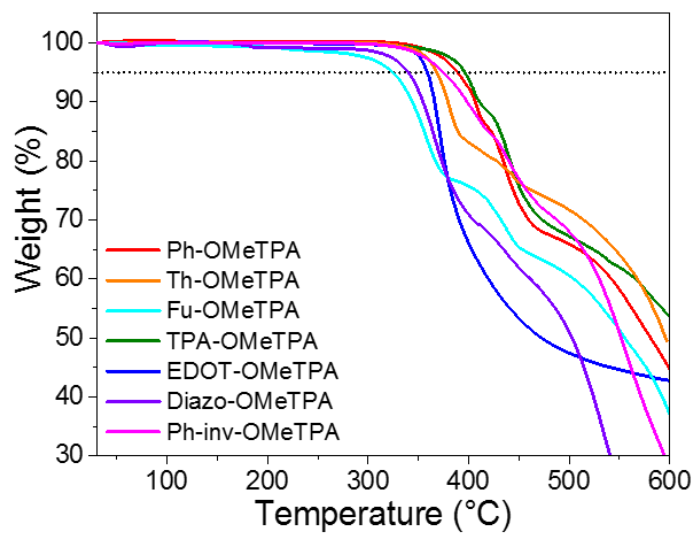


Figure S 2. TGA thermograms of the azomethine-based small molecules at a heating rate of $10\text{ }^{\circ}\text{C min}^{-1}$ under nitrogen.

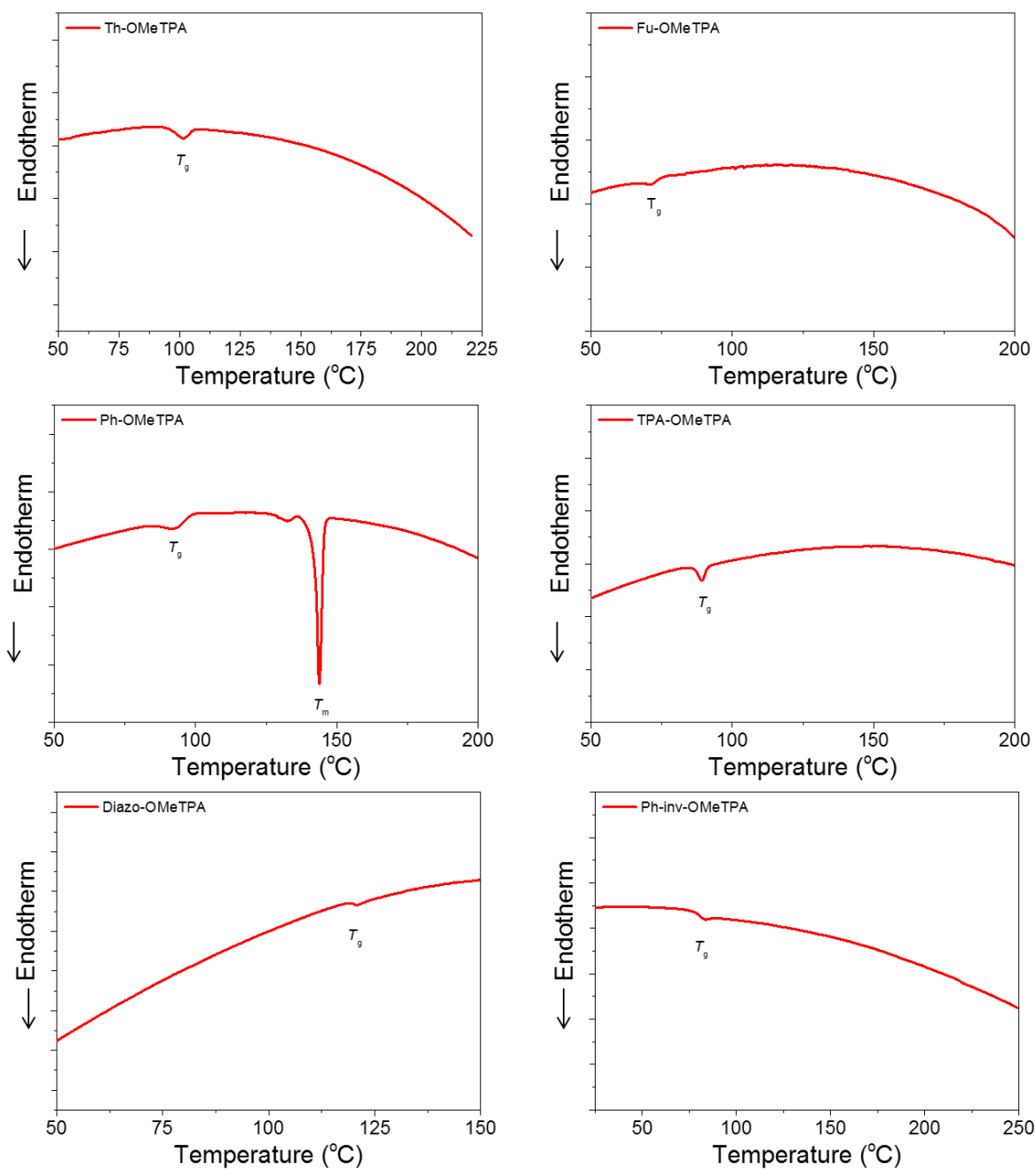


Figure S 3. DSC curves of the azomethine based small molecules at a heating rate of 20 °C min⁻¹ under nitrogen. Measurements obtained from the first heating ramp.

4 Optoelectronic properties

4.1 UV-Vis spectroscopy

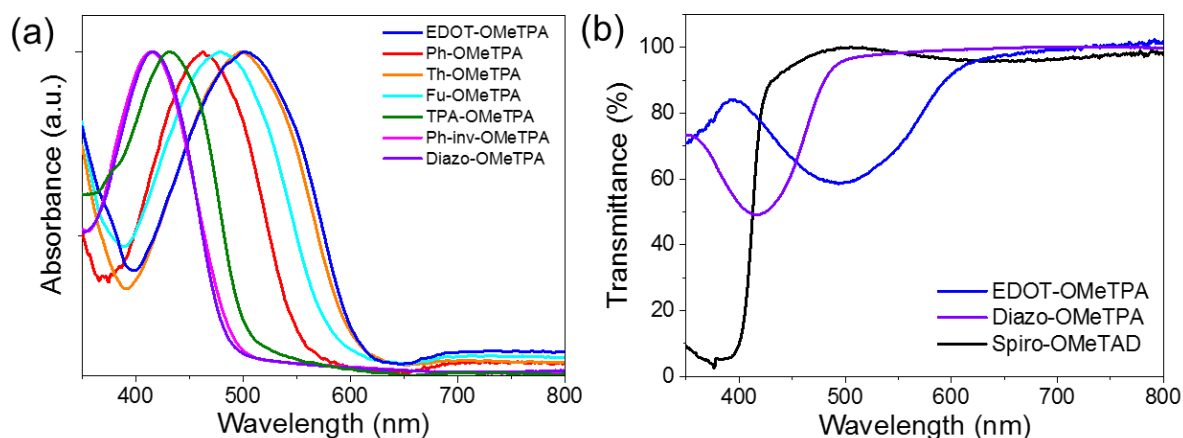


Figure S 4. (a) Normalized UV-Vis absorption spectra of the azomethine-based HTMs in the solid state. The materials were spincoated from chlorobenzene at a concentration of 10 mg mL^{-1} on glass substrates coated with a thin compact layer of Al_2O_3 . (b) The transmittance two azomethine-based HTMs and Spiro-OMeTAD ($\sim 250 \text{ nm}$) as a reference.

Table S 12. Optical properties of the HTMs obtained from UV-Vis, the bandgap was obtained from the absorption onset.

Compound	$\lambda_{\text{max, solution}} \text{ (nm)}$	$\lambda_{\text{max, film}} \text{ (nm)}$	$\lambda_{\text{onset, film}} \text{ (nm)}$	$E_g \text{ (eV)}$
EDOT-OMeTPA	501	507	625	1.98
Ph-OMeTPA	457	466	553	2.24
Th-OMeTPA	492	500	605	2.05
Fu-OMeTPA	472	482	583	2.13
TPA-OMeTPA	430	434	507	2.45
Ph-inv-OMeTPA	415	416	490	2.53
Diazo-OMeTPA	419	417	483	2.57

4.1.1 Oxidation with LiTFSI

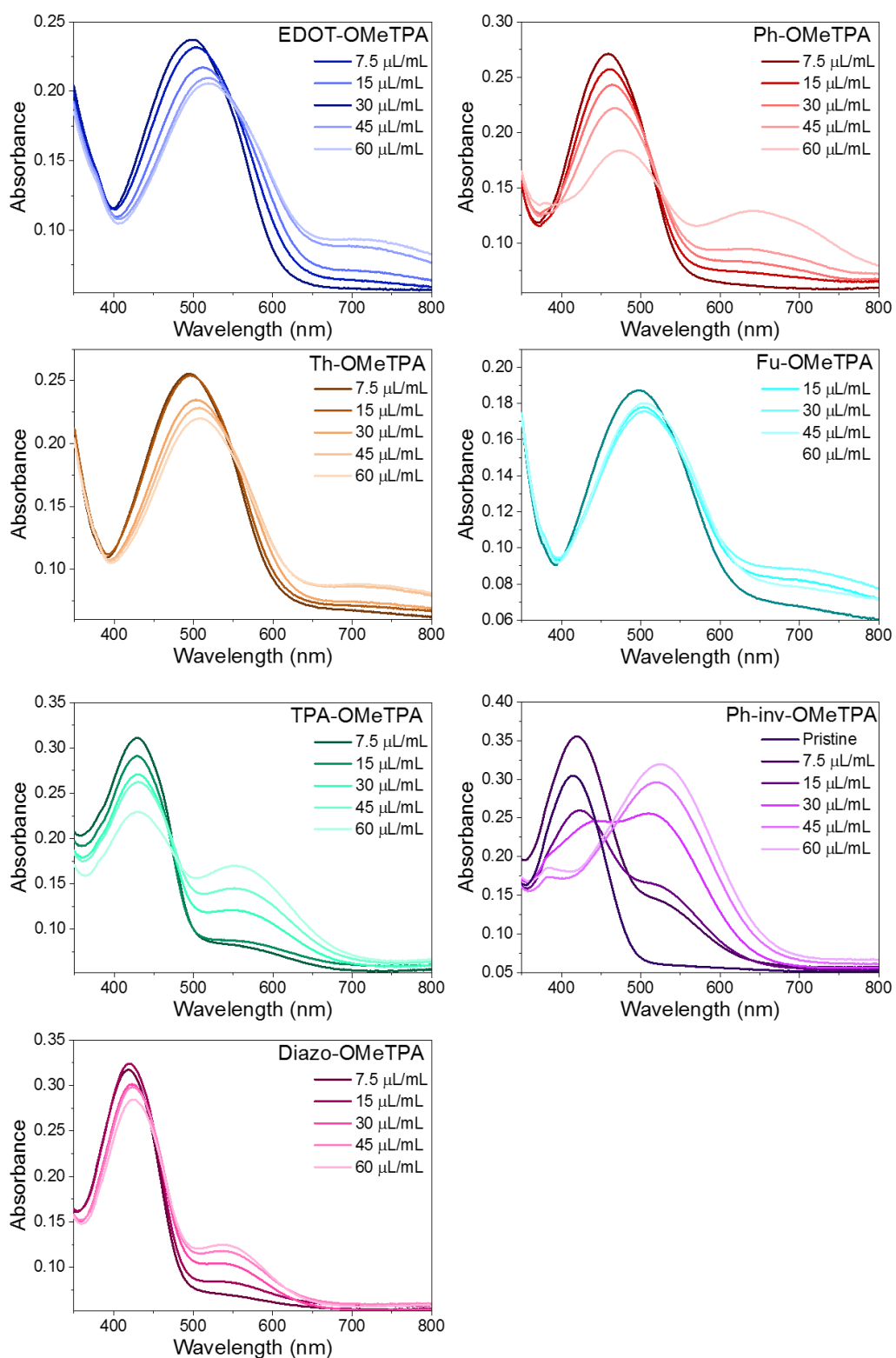


Figure S 5. UV-Vis spectra of thin HTM films prepared from solutions containing different amounts of LiTFSI (170 mg/mL) as oxidant. All films were stored for 24 h under air (< 30% R.H.) before measuring. An absorption peak attributed to the oxidized species is observed with a redshift compared to the pristine material.

4.2 Cyclic voltammetry

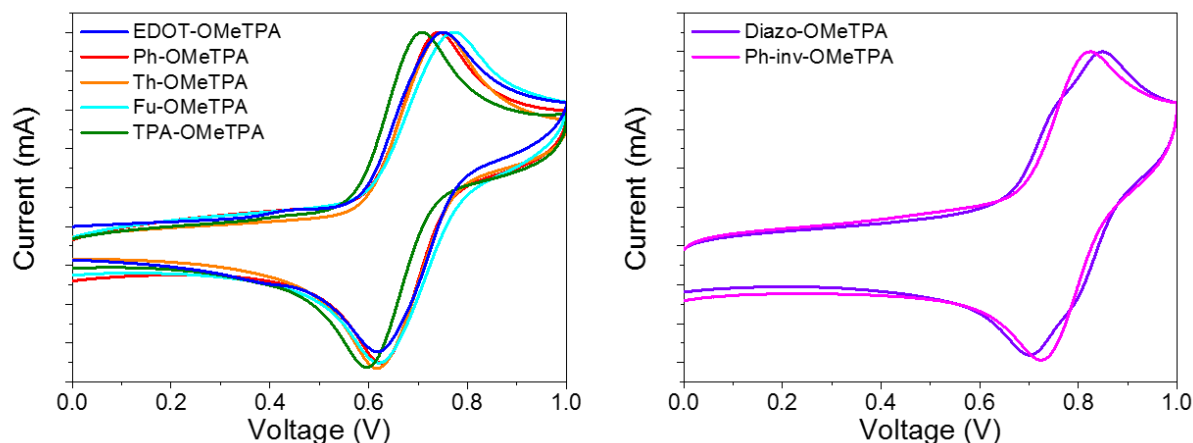


Figure S 6. Cyclic voltammograms of the azomethine-based HTMs measured in a dichloromethane solution containing $t\text{BuNPF}_6$ as electrolyte. Oxidation potential is measured vs. Ag/Ag^+ . Left graph showing HTMs with the standard azomethine bond, right HTMs with the inverted azomethine bond.

Table S 13. Energy levels obtained from cyclic voltammetry

Compound	HOMO _{exp.} (eV)	LUMO _{exp.} (eV) ^a	E_g exp. (eV)
EDOT-OMeTPA	-5.28	-3.3	1.98
Ph-OMeTPA	-5.30	-3.1	2.24
Th-OMeTPA	-5.30	-3.3	2.05
Fu-OMeTPA	-5.30	-3.2	2.13
TPA-OMeTPA	-5.28	-2.8	2.45
Ph-inv-OMeTPA	-5.39	-2.9	2.53
Diazo-OMeTPA	-5.36	-2.8	2.57

^a estimated by adding the optical bandgap to the HOMO energy level

4.3 Computational studies

Table S 14. Energy levels obtained from DFT calculations in vacuum.

Compound	HOMO _{DFT} (eV)	LUMO _{DFT} (eV)	E_g DFT (eV)
EDOT-OMeTPA	-4.37	-1.95	2.42
Ph-OMeTPA	-4.52	-1.91	2.61
Th-OMeTPA	-4.47	-2.04	2.43
Fu-OMeTPA	-4.42	-1.85	2.57
TPA-OMeTPA	-4.45	-1.56	2.89
Ph-inv-OMeTPA	-4.59	-1.46	3.13
Diazo-OMeTPA	-4.49	-1.40	3.09

5 Hole mobility

The high work function of the MoO_x electrodes makes it possible to selectively collect holes. The current-voltage characteristics were recorded in the dark. At higher voltages, assuming ohmic injecting contacts and trap-free transport, the current measured is space-charge limited. The charge carrier mobility can be estimated by using the Mott-Gurney equation.^[S12]

$$J = \frac{9}{8} \epsilon_0 \epsilon_r \mu \frac{V^2}{L^3}$$

where J is the current density, ϵ_r is the dielectric constant of the organic semiconductor blend (assumed to be 3 in our calculations), ϵ_0 is the permittivity of free space, μ is the charge carrier mobility, L is the thickness of the active layer and V is the voltage drop across the device.

The charge mobility of the HTMs with the azomethine-bond in the standard orientation shows a field dependence which can be described with the Poole-Frenkel effect.^[S11]

$$\mu(E) = \mu_0 \exp(\gamma \sqrt{E}),$$

where μ_0 is the zero-field hole mobility, γ the field coefficient and E the electric field, which was stated as:

$$E = \frac{V}{L}$$

The electric field was considered to be constant along the active layer thickness.

The values of γ and μ_0 were obtained by fitting equations to find a best fit with the experimental data. Details for deriving these equations are published by Murgatroyd.^[S12]

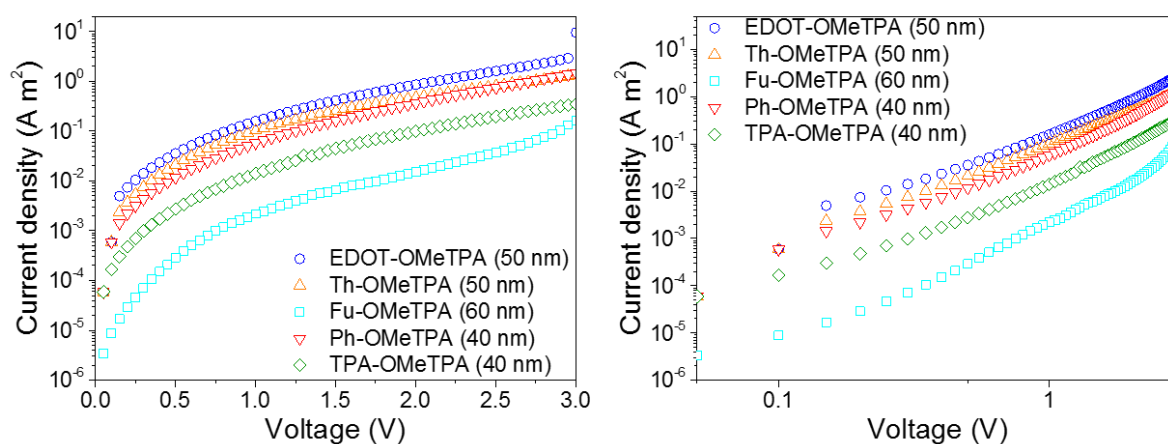


Figure S 7. Linear-logarithmic and logarithmic-logarithmic voltage-current density plots to determine the field-dependent mobility of the azomethine-based HTMs by fitting the equation for the space-charge limited current. The layer thicknesses are added to the legend.

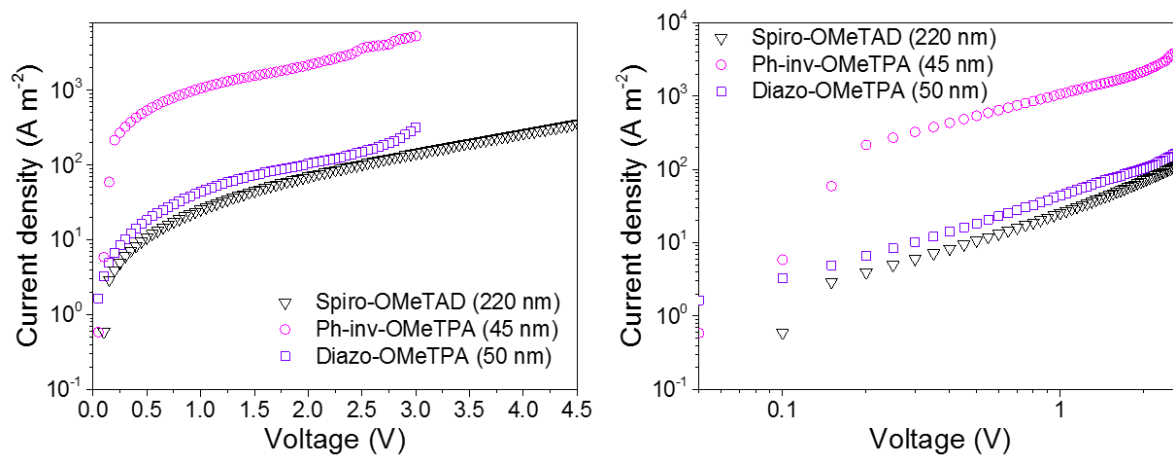


Figure S 8. Linear-logarithmic and logarithmic-logarithmic voltage-current density plots to determine the field-dependent mobility of the azomethine-based HTMs by fitting the equation for the space-charge limited current. Spiro-OMeTAD was added as a reference and the layer thicknesses are added to the legend.

6 Solar cell performance

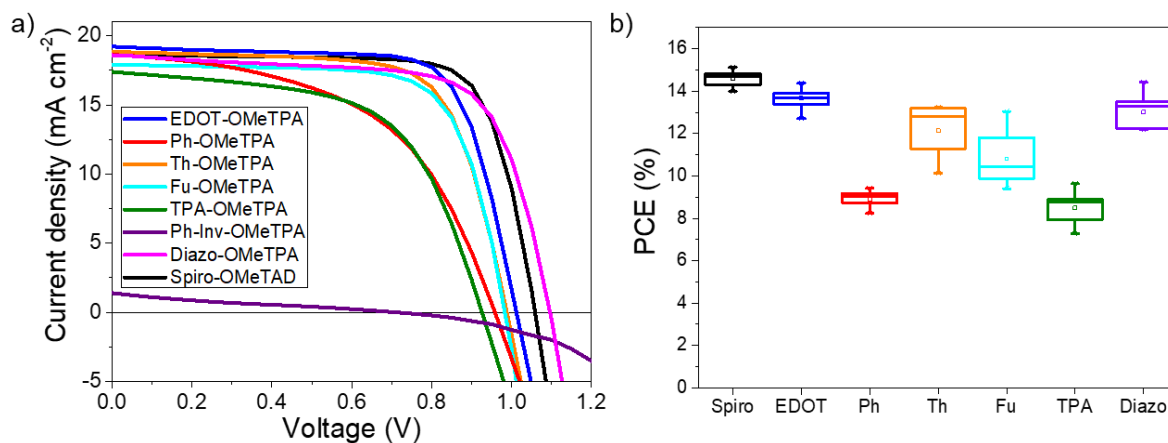


Figure S 9. Photovoltaic characterization. a) J-V curves of the perovskite solar cells comprising the different HTMs. b) Box-diagram showing the distribution of the performance of 9 individual devices.

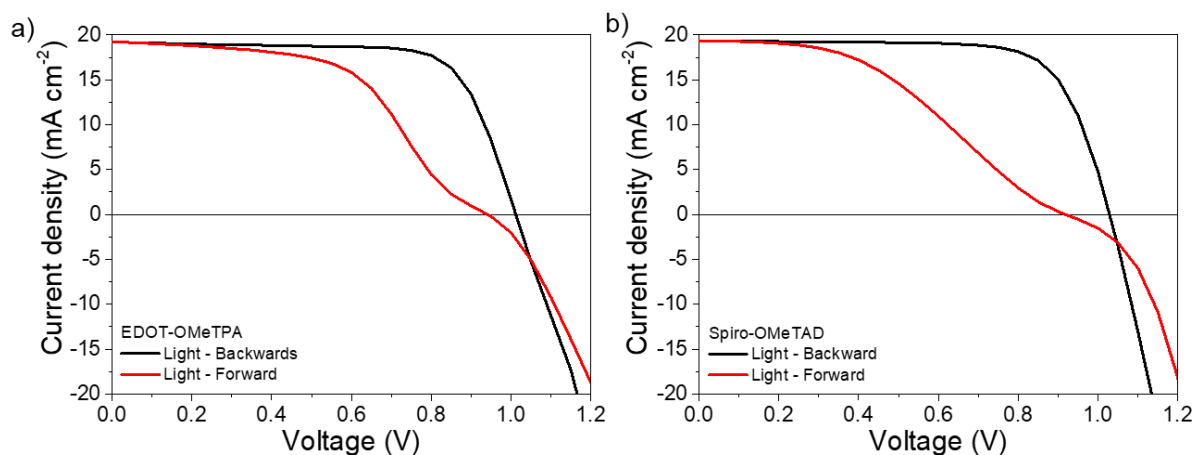


Figure S 10. Photovoltaic characterization. Typical hysteresis in these devices. We assign the hysteresis to the perovskite and/or electron transporting layer, rather than the HTM.

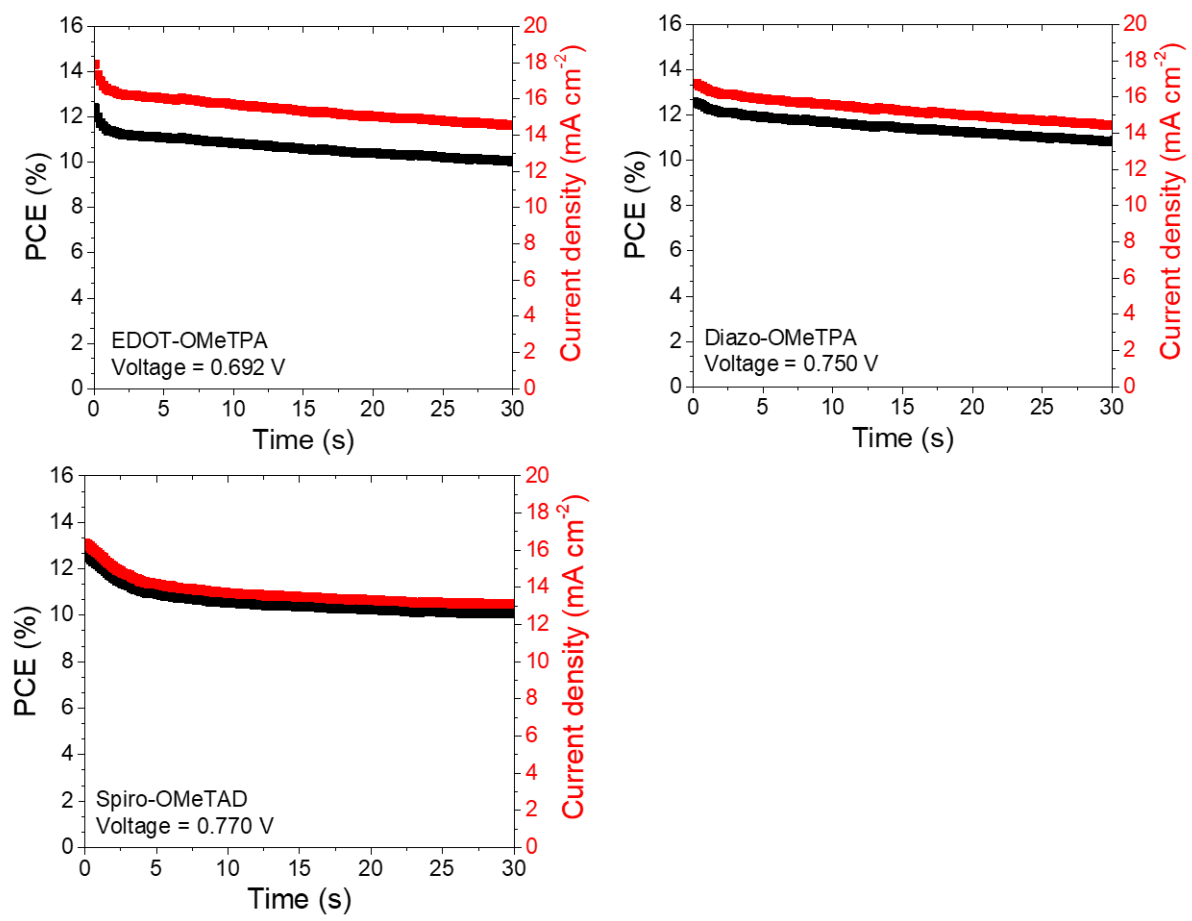


Figure S 11. Power conversion efficiency and current density as a function of time under operating conditions of solar cells comprising the two most efficient azomethine-based hole-transporting materials.

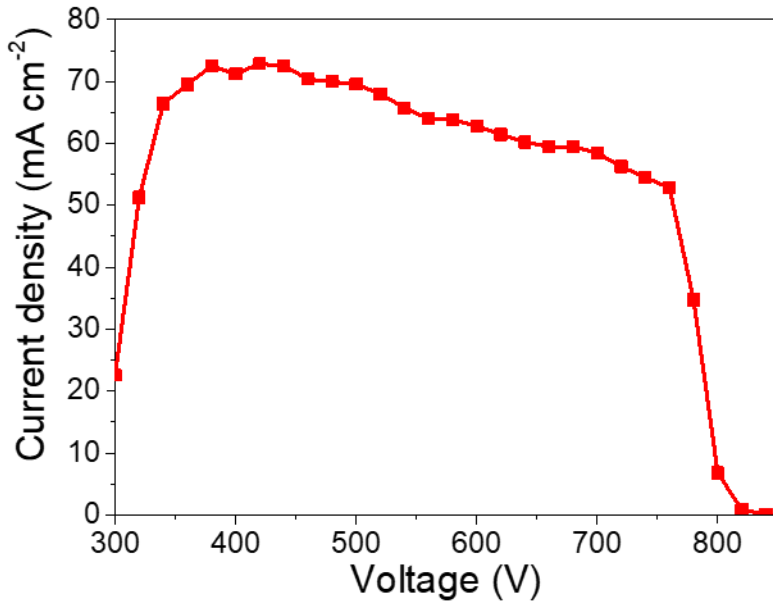


Figure S 12. External quantum efficiency spectrum of a device based on MAPbI₃.

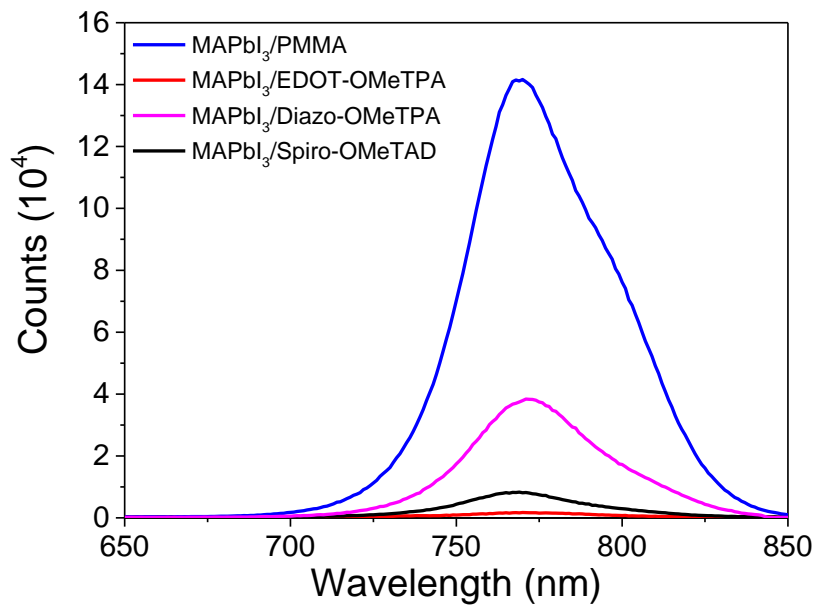


Figure S 13. Photoluminescence emission scans for the neat MAPbI₃ and bilayer samples.

7 Moisture barrier properties

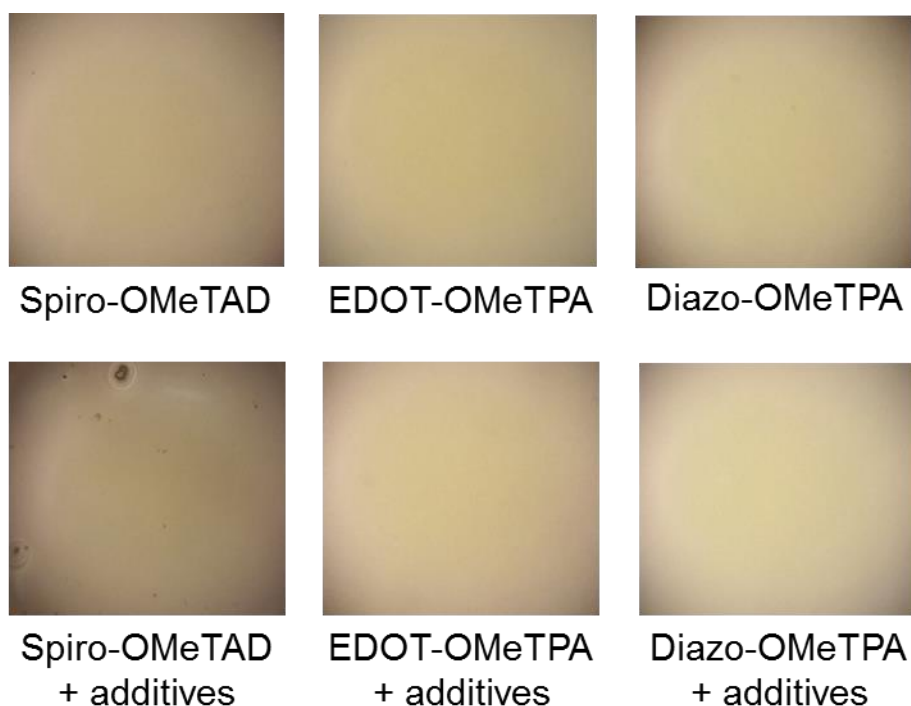


Figure S 14. Light microscopy images of pristine HTM films and films prepared with the additives LiTFSI and tBP. All pristine films look smooth and mostly defect and pinhole free. Upon addition of the additives (used at the same amount as used for the preparation of photovoltaic devices), the quality of the Spiro-OMeTAD film is significantly reduced, which is in agreement with literature,^{S13} while the azomethine-based HTMs still show high quality films.

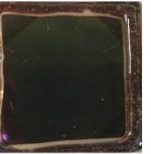
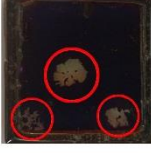
Material	0 h	8 h	24 h	14 days
EDOT-OMeTPA				
Ph-OMeTPA				
Th-OMeTPA				
Fu-OMeTPA				
TPA-OMeTPA				
Ph-inv-OMeTPA				
Diazo-OMeTPA				
Spiro-OMeTAD				

Figure S 15. Photographs of $\text{CH}_3\text{NH}_3\text{PbI}_3$ perovskite films covered with a layer of the HTMs stored at 75% RH. The decolouration, which is clearly observed for the sample with Spiro-OMeTAD, is attributed to the degradation of the perovskite. For the azomethine-based films, degradation starts from the epoxy-covered edge of the samples.

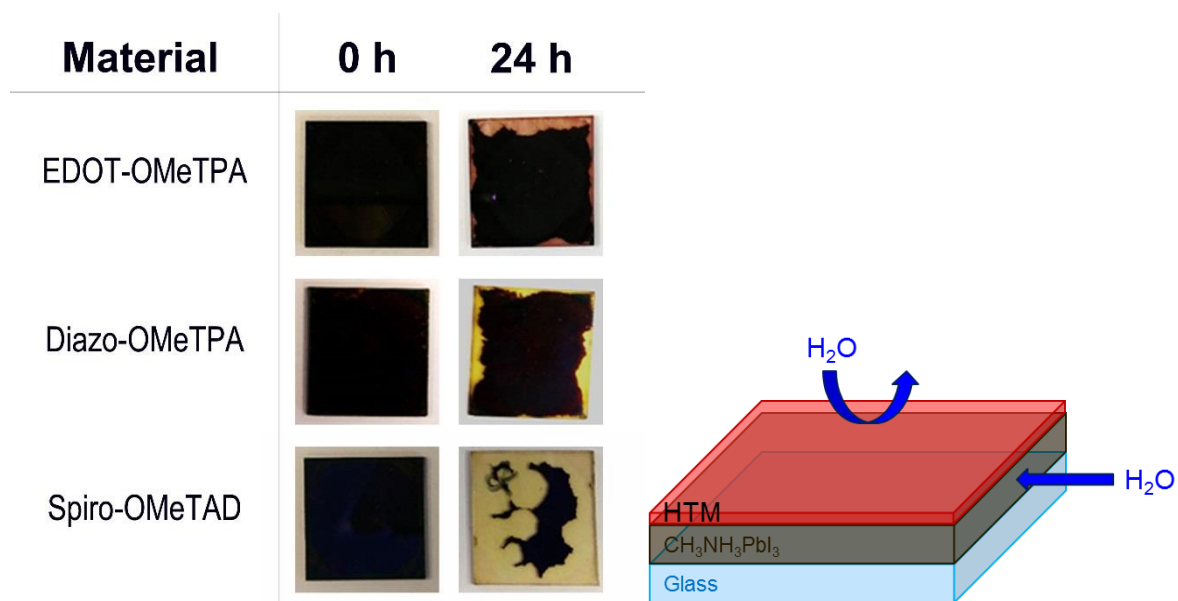


Figure S 16. Photographs of $\text{CH}_3\text{NH}_3\text{PbI}_3$ perovskite films covered with a layer of the HTMs stored at 75% RH, without covering the edges with epoxy. Clearly all samples degrade from the edge inwards, as is depicted in the schematic representation on the right. Nevertheless, here we also observe that the Spiro-OMeTAD sample degrades significantly faster.

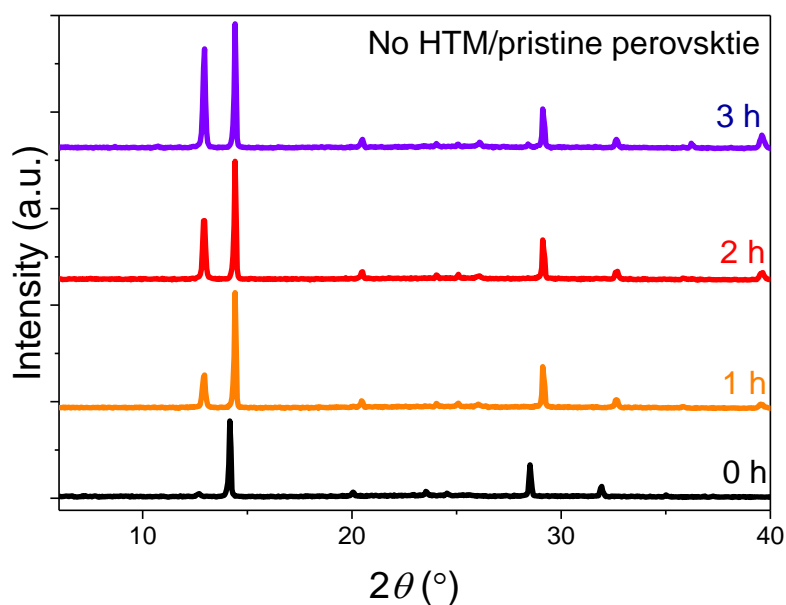


Figure S 17. XRD patterns obtained from in-situ hydration measurements of the pristine perovskite at 90% RH. The reflection from PbI_2 , which is the degradation product of the perovskite, is indicated with an asterisk. The perovskite is prepared using 5% PbI_2 excess in the precursor solution, which explains the initial small PbI_2 peak. The pristine sample degrades faster than all bilayer films.

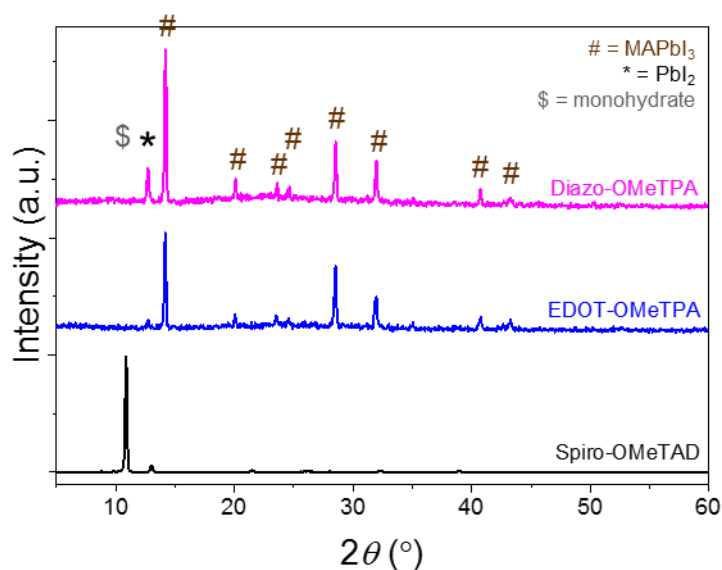


Figure S 18. XRD patterns obtained from HTM-perovskite bilayers after hydration for 30 days at 75% RH (same films as in Figure 6). The edges of the films were covered with epoxy to prevent moisture-induced degradation from the side. The perovskite was prepared using 5% PbI_2 excess in the precursor solution, however, a small increase in the PbI_2 peak is observed for the **Diazo-OMeTPA** sample, while the bilayer with **EDOT-OMeTPA** does not show any degradation. This is in strong contrast with the bilayers containing Spiro-OMeTAD, where the perovskite is complete degraded, and only the monohydrated species and a small PbI_2 peak are observed, confirming the origin of the colour loss of the film.

8 References

- [S1] M. L. Petrus, F. S. F. Morgenstern, A. Sadhanala, R. H. Friend, N. C. Greenham, T. J. Dingemans, *Chem. Mater.* **2015**, *27*, 2990–2997.
- [S2] M. L. Petrus, T. Bein, T. J. Dingemans, P. Docampo, *J. Mater. Chem. A* **2015**, *3*, 12159–12162.
- [S3] B.-B. Ma, H. Zhang, Y. Wang, Y.-X. Peng, W. Huang, M.-K. Wang, Y. Shen, *J. Mater. Chem. C* **2015**, *3*, 7748–7755.
- [S4] M. L. Petrus, Y. Hu, D. Moia, P. Calado, A. M. A. Leguy, P. R. F. Barnes, P. Docampo, *ChemSusChem* **2016**, *9*, 2699–2707.
- [S5] M. Yano, Y. Ishida, K. Aoyama, M. Tatsumi, K. Sato, D. Shiomi, A. Ichimura, T. Takui, *Synth. Met.* **2003**, *137*, 1275–1276.
- [S6] C.-W. Chang, G.-S. Liou, *J. Mater. Chem.* **2008**, *18*, 5638–5646.
- [S7] M. A. Topchiy, P. B. Dzhevakov, M. S. Rubina, O. S. Morozov, A. F. Asachenko, M. S. Nechaev, *European J. Org. Chem.* **2016**, *2016*, 1908–1914.
- [S8] J. Zeng, T. Zhang, X. Zang, D. Kuang, H. Meier, D. Cao, *Sci. China Chem.* **2013**, *56*, 505–513.
- [S9] S. M. Budy, S. Suresh, B. K. Spraul, D. W. Smith, *J. Phys. Chem. C* **2008**, *112*, 8099–8104.
- [S10] D. Shi, Y. Cao, N. Pootrakulchote, Z. Yi, M. Xu, S. M. Zakeeruddin, M. Grätzel, P. Wang, *J. Phys. Chem. C* **2008**, *112*, 17478–17485.
- [S11] P. W. M. Blom, M. J. M. De Jong, M. G. Van Munster, *Phys. Rev. B* **1997**, *55*, 656–659.
- [S12] P. N. Murgatroyd, *J. Phys. D Appl. Phys.* **1970**, *3*, 151–156.
- [S13] I. Lee, J. H. Yun, H. J. Son, T.-S. Kim, *ACS Appl. Mater. Interfaces* **2017**, *9*, 7029–7035.
- [S14] B.-B. Ma, H. Zhang, Y. Wang, Y.-X. Peng, W. Huang, M.-K. Wang, Y. Shen, *J. Mater. Chem. C* **2015**, *3*, 7748–7755